Chemical Engineering Journal 162 (2010) 380–387

Contents lists available at ScienceDirect

Chemical Engineering Journal

journal homepage: www.elsevier.com/locate/cej

Total oxidation of toluene over metal oxides supported on a natural clinoptilolite-type zeolite

Gülin S. Pozan Soylu*, Zeynep Özçelik, İsmail Boz

Istanbul University, Faculty of Engineering, Chemical Engineering Department, Avcilar Campus, Avcilar, 34320 Istanbul, Turkey

ARTICLE INFO

Article history:
Received 12 March 2010
Received in revised form 7 May 2010
Accepted 12 May 2010

Keywords:
Catalytic oxidation
Toluene
Transition metals
Clinoptilolite
Acidity
Characterization

ABSTRACT

Some selected (Mn^{2+}, Co^{2+}, Fe^{3+}, Cu^{2+}) oxides supported on clinoptilolite were tested in the catalytic incineration of toluene. Manganese oxide on clinoptilolite was found to be the most active and durable of all tested. The effects of ion exchanger concentration, ion exchange time, ion exchange temperature and the type of ion exchanger were also studied to screen metal oxide catalysts. The catalysts were prepared by incipient wetness impregnation of clinoptilolite in hydrogen form (HCLT). They were characterized by X-ray diffraction (XRD), scanning electron microscopy (SEM), temperature-programmed reduction/oxidation (TPR/TPO) and diffuse reflectance Fourier transform infrared (DRIFT) spectroscopy techniques. Activities of the candidate catalysts were correlated with crystallinity, surface acidity, adsorption properties and morphological parameters. 9.5% MnO_2 on clinoptilolite exhibits the highest performance among the different oxides. Its higher activity was attributed to its ability to maintain its redox potential. Furthermore, this novel generation of catalysts appeared as active as conventional ZSM-5 and BETA. Finally, it was found that all four metal oxides supported on clinoptilolite led to the considerable decrease in combustion temperature.

1. Introduction

Volatile organic compounds (VOCs) are not only major contributors to air pollution but also as main precursors of ozone and smog formation [1–3]. In many countries, including USA, EU, Japan and Korea, stringent legislations have been put in effect to abate VOCs emission. It is also widely recognized that catalytic oxidation was a viable method of controlling emissions of VOCs owing to its low thermal NO_x emissions, low operating cost, and high destruction efficiency [4,5]. The function of catalysts was to convert the VOCs into relatively harmless compounds at lower operating temperatures [6,7]. Supported precious metals such as Pt and Pd have been well established as efficient catalysts for VOCs catalytic combustion [8]. However, the quest for cheaper and more environmentally friendly catalytic materials, thus avoiding problems of costly precious metal waste and recovery [9,10], can be answered by utilizing non-precious metal oxides.

The transition metal oxides catalysts were associated with their lower cost as well as possible higher thermal stability, resistance to humidity, specific surface area, ability to stabilize the metal particles in the porous structure [8,11]. The catalytic combustion of toluene has been studied with catalysts including zeolite-based metal oxides [3,12,13].

Zeolites were renowned as promising supports to stabilize transition metals with great potential as oxidation catalysts [14]. The availability of zeolites with several porous structures, different composition and hydrophobicity degree, as well as the possibility to control the acidic properties and location of exchanged cations have contributed to the increased usage of zeolites [15]. HY and HZSM-5 (HMFI) zeolites exchanged with copper (1–5 wt.%) and cesium (5–10 wt.%) have been studied as catalysts for the combustion of toluene [3].

Most of the studies in this area were concentrated on the use of clinoptilolite in the removal of ammonium ions related to its significant selectivity [16,17]. Clinoptilolite is a natural zeolite with the formula $(Na_2,K_2,Ca)_3Al_6Si_{30}O_{72}\cdot 24H_2O$. The chemical composition of clinoptilolite was characterized by the remarkable variations in the Si/Al ratio as well as in the composition of the exchangeable cations [18,19].

In this work, clinoptilolite was selected as the catalyst support due to its microporous structure and high thermal stability. The chosen probe molecule was toluene, which was a common solvent in chemical and processing industries and also was an important POCP (Photochemical Ozone Creativity Potential) [2,3]. The objective of the present work was to examine the selected metal (Mn^{2+}, Co^{2+}, Fe^{3+}, Cu^{2+}) oxides supported on clinoptilolite, which was modified by ion exchange in the catalytic combustion of toluene in air.

* Corresponding author. Tel.: +90 212 473 70 70x17789; fax: +90 212 473 71 80.
E-mail address: gpozan@istanbul.edu.tr (G.S.P. Soylu).

1385-8947/$ – see front matter © 2010 Elsevier B.V. All rights reserved.
doi:10.1016/j.cej.2010.05.020

Table 1
Physicochemical properties of the natural clinoptilolite.

Chemical composition (w/w)	SiO_2 72%, Al_2O_3 12%, Fe_2O_3 1.90%, TiO_2 0.10% CaO 3.7%, MgO 1.2%, Na_2O 0.65%, K_2O 3.5% Mn 0.08%, SiO_2/Al_2O_3, 5.8%
Mineralogical composition	Clinoptilolite (88–95%), feldspar (3–5%) montmorillonite (2–5%), muscovite (0–3%) cristobalite (0–2%)
Physical properties	BET surface area: 39 $m^2\ g^{-1}$ Total exchange capacity: 2.73 meq/g (calculated as the sum of Mg, Ca, K and Na cations) pH 7.85 particle density = 2.27 $g\ cm^{-3}$

2. Materials and methods

2.1. Catalyst preparation

Clinoptilolite-rich mineral was obtained from the Gördes deposit in Aegean Sea of Turkey. The clinoptilolite-rich mineral from Gördes was characterized by using X-ray diffraction (XRD), scanning electron microscopy (SEM) and thermal analysis techniques (TGA–DTA). The SEM pictures of some clinoptilolite samples are well correlated with the literature data. The physicochemical properties of the natural clinoptilolite are given in Table 1.

The total exchange capacity of Gördes clinoptilolite was well consistent with those found for other two clinoptilolite samples from nearby regions, a Greek clinoptilolite of 2.62 meq/g and a Bigadic clinoptilolite of Turkey of 2.62 meq/g [11,20,21].

Clinoptilolite samples were treated with 1 M NaCl, 1 M NH_4NO_3 and 1 M NH_4Cl solution at 70 °C in water bath shaker for 1.5, 6, 12, 24, 48 and 72 h. Then, clinoptilolite was separated by centrifuging at 4000 rpm. Clinoptilolite samples were washed with deionized water several times until all traces of chlorine anions were removed. Samples were dried in oven at 110 °C for 16 h. Clinoptilolites were converted to H form by calcining in air at 550 °C for 4 h. Initial and final concentrations of the exchanging cations and sodium were determined.

Two alternative zeolites, NH_4ZSM-5 (SiO_2/Al_2O_3 = 30, BET surface area of 400 m^2/g) and NH_4BETA (SiO_2/Al_2O_3 = 25, BET surface area of 680 m^2/g) available in the interval 40/60 mesh, have also been used for comparison purposes. NH_4ZSM-5 and NH_4BETA were prepared by treating commercial ZSM-5 and Beta samples with 0.1 M NH_4Cl solution at 30 °C in a water bath shaker for 2 h. NH_4ZSM-5 and NH_4BETA zeolites were used after calcination at 500 °C for 4 h to convert into HZSM-5 and H-BETA form.

Transition metal solutions (0.25 M) were prepared by dissolving $Co(NO_3)_2{\cdot}6H_2O$ (Merck), $Fe(NO_3)_3{\cdot}9H_2O$, $Mn(NO_3)_2{\cdot}4H_2O$ (Merck) (Merck) and of $Cu(NO_3)_2{\cdot}3H_2O$ in distilled water. Catalysts containing nitrates of Co, Fe, Mn, and Cu metals were prepared by incipient wetness impregnation of ion exchanged zeolites. The impregnated support was dried at 105 °C for 14 h, and it was calcined in air at 500 °C for 4 h. The resultant metal oxide loaded clinoptilolite was ground at a constant vibration rate of 300 rpm for 15 min in a Retsch MM 200 vibrant-ball mill by 12 mm ZrO_2 milling ball in ZrO_2 milling container. Particulate size of 53–90 μm was sieved and used in activity tests. In addition, MnO_2 (>99%) was purchased from Riedel-De Haen Chemical Co. and used as received for comparison purposes. Metal oxide loading of the catalysts was nominally 3, 5, 9.5, 12 and 20 wt.% and reported as the weight percentages of their common oxides, Co_2O_3, Fe_2O_3, CuO and MnO_2. For instance, $9.5MnO_2$/HCLT means that the catalyst contained nominally 9.5% MnO_2 by weight and deposited on to HCLT support.

2.2. Characterization techniques

The composition of the catalyst was determined using Thermo Elemental X Series ICP-MS and Varian Spectra Fast Sequential-220 atomic absorption spectrometer with an air–acetylene flame. Actual metal concentrations were listed in Table 2.

Surface area and pore size distribution were measured using a Costech sorptometer 1042 equipment using low temperature N_2 adsorption. Results were obtained after drying the samples in situ at 200 °C for 4 h.

Powder X-ray diffractions of samples were obtained using a Rigaku D/Max-2200 diffractometer with the CuKα (λ = 1.540) radiation. Samples were scanned from 10 to 80 at a rate of 2°/min (in 2Θ). The sizes of the crystalline domains were calculated by using the Scherer equation, $t = C\lambda/B\cos\Theta$, where λ is the X-ray wavelength (A°), B is the full width at half maximum, Θ is Bragg angle, C is a factor depending on crystallite shape (taken to be one), and t is the crystallite size (A°). Relative crystallinity was calculated on the basis of comparing the average intensities for most intense peaks for the parent vs. treated zeolite catalyst.

By using Xpowder program, line broadening has been taken into account. The variation of the FWHM of the peaks is generally described by the Caglioti equation, values found after such correction were calculated and tabulated in.

Diffraction theory predicts that the diffraction lines of a XRD powder pattern will be very sharp for a crystalline material consisting of sufficiently large and strain-free crystallites, therefore, the XRD line broadening (peak width) inversely correlates with crystal size and lattice perfection.

The relative intensities were determined as diffraction line heights relative to the most intense line normalized to the intensity of 100, Rigaku software. The position of reference silicon diffraction line was determined with Rigaku software using pseudo-Voigt profile function. The angular width (B, FWHM) was corrected for instrumental line broadening by using Caglioti function. The reciprocal of the B value ($1/B$) correlates to the crystallite size/perfection.

Table 2
Metal oxide content, Crystallite size, Crystallinity of catalysts, BET surface area, H_2 and O_2 consumption values of catalysts in TPR/TPO analysis.

Catalyst (metal oxide/zeolite)	Metal oxide content (wt.%)	Crystallite size (nm)	Crystallinity (%)	BET surface area ($m^2\ g^{-1}$)	mmol H_2/g_{cat}	mmol O_2/g_{cat}
$9.5Fe_2O_3$/HCLT	$9.40Fe_2O_3$	39	90	258	0.246	0.115
$9.5Co_3O_4$/HCLT	$9.45Co_3O_4$	41	92	181	0.270	0.121
$3MnO_2$/HCLT	$2.79MnO_2$	21	75	158		
$5MnO_2$/HCLT	$4.88MnO_2$	40	89	106		
$9.5MnO_2$/HCLT	$9.46MnO_2$	78	93	54	0.407	0.195
$12MnO_2$/HCLT	$11.95MnO_2$	80	94	43		
$20MnO_2$/HCLT	$19.94MnO_2$	82	94	32		
9.5CuO/HCLT	9.46CuO	76	91	63	0.365	0.164
$9.5MnO_2$/H-Beta	$9.45MnO_2$	77	92	154	0.265	0.117
$9.5MnO_2$/HZSM-5	$9.42MnO_2$	40	90	388	0.154	0.063
HCLT				225		

Table 3
T_{50}, T_{90} and T_{100} values, ignition temperature at maximum conversion to CO_2.

Catalyst (metal oxide/zeolite)	T_{50}	T_{90}	T_{100}	T (°C) (CO_2(max)%)
9.5Fe_2O_3/HCLT	333	–	–	–
9.5Co_3O_4/HCLT	321	–	–	–
3MnO_2/HCLT	376	–	–	550 (86)
5MnO_2/HCLT	328	–	–	500 (76)
9.5MnO_2/HCLT	272	297	350	350 (100)
12MnO_2/HCLT	278	389	550	550 (100)
20MnO_2/HCLT	322	–	–	550 (67)
9.5CuO/HCLT	330	401	550	550 (100)
9.5MnO_2/HZSM-5	323	–	–	550 (65)
9.5MnO_2/H-Beta	314	350	500	478 (100)
MnO_2	329	441	550	550 (100)
HCLT	342	–	–	550 (76)
9.5MnO_2/NaCLT (1 M NaCl – 70 °C – 48h)	272	345	400	400 (100)
9.5MnO_2/HCLT (1 M NH_4Cl – 70 °C – 48h)	275	296	350	350 (100)
9.5MnO_2/HCLT (1 M NH_4NO_3 – 70 °C – 48 h)	266	292	350	300 (100)

The morphology of clinoptilolite was determined by Scanning Electron Microscopy (JEOL-5600 SEM −30 kV electron beam).

Thermo gravimetric (TG) analysis was performed using a Shimadzu TGA-60WS thermo gravimetric analyzer. All the samples were heated from 30 to 1000 °C with a heating rate of 10 °C/min using approximately 15 mg of sample powder under flowing air (50 ml/min). The decomposition behavior and weight loss steps were observed in TG/DTG curves.

Temperature-programmed reduction (TPR) was performed to monitor the reduction of the metal oxide while the temperature increased from 60 to 600 °C. TPR profiles were obtained by using Quantachrome ChemBET 3000 flow type equipment. In TPR experiments, 60 mg of the catalyst was dried at 105 °C for 2 h, and 10% H_2/N_2 (BOS, 99.99% purity) was used as a reducing gas. Temperature ramp rate was 10 °C/min and flow rate was 70 ml/min. The changes in H_2 flow were followed using a thermal conductivity detector.

Recording successive reduction/oxidation cycles helped in monitoring the compositional stability during the prolonged use of a catalyst. TPO profile was obtained by using Quantachrome ChemBET 3000 flow type equipment. After TPR experiments, the reduced sample were oxidized using air with a flow rate of 70 ml/min, increasing the temperature from room temperature to 600 °C at a heating rate of 10 °C/min.

Diffuse reflectance Fourier transform infrared (DRIFT) spectra of adsorbed ammonium were recorded with a Nicolet 380 spectrometer, equipped with an environment controlled-diffuse reflectance chamber and signals were collected using a water-cooled DTGS detector. Spectra were collected in the range of 4000–1000 cm^{-1} averaging 200 scans at an instrumental resolution of 4 cm^{-1}, and analyzed with OMMIC software. Before adsorbing ammonium at room temperature, thin catalyst wafer was heated at 500 °C and then kept under flowing Helium at 500 °C for 1 h. After the sample was treated in flowing 5000 ppm NH_3/He at 30 °C for 30 min and then the FT-IR spectra of ammonium absorbed on the catalysts were recorded under flowing He at an increasing temperature from room temperature to 400 °C.

The acidic properties of catalysts were investigated by *n*-butylamine desorption using a Shimadzu TGA-60WS thermo gravimetric analyzer. Catalysts were treated with *n*-butylamine vapors in a desiccators for adsorption and then the weight loss curves of adsorbed *n*-butylamine were recorded by TGA at the heating rate of 10 °C min^{-1}.

2.3. Catalytic activity

Catalytic activity was determined in a fixed-bed reactor, in which typically 0.15 g of catalyst was utilized in glass wool packing. Prior to catalytic tests, catalyst precursors were heated in the flowing air at 500 °C with the rate of 10 °C/min, and kept at 500 °C for 1 h. Catalytic activity of the calcined samples was measured by the total combustion of the toluene in air. The reaction feed consisted of 1000 ppm toluene balance being dry air. The feed stream to the reactor was prepared by delivering toluene using a syringe pump (Cole Palmer 74900-05) into dry air, which was metered by a mass flow controller (Brooks, 5850TR). A fixed gas hourly space velocity of 15,000 h^{-1} was used for all studies. Catalytic activity was measured over the range 150–550 °C, and temperatures were measured by a thermocouple placed just beneath the catalyst bed. Conversion data were calculated by the differentiating between inlet and outlet concentrations. In order to determine the catalytic activity of the catalysts, T_{50} and T_{90} values were calculated from light-off curves. T_{50} was defined as temperature at which 50% conversion of toluene was attained. Conversion measurements and product profiles were taken at steady state, typically after 30 min on stream. The feed and effluent streams were analyzed by on-line gas chromatograph (HP 6890+) equipped with a thermal conductivity detector (TCD) and a flame ionization detector (FID) in series. The hydrocarbons and carbon dioxide were analyzed with a Poraplot Q capillary column (30 m × 0.530 mm × 40 μm) and carbon monoxide with a Molecular Sieve 5A capillary column (30 m × 0.530 mm × 50 μm), both columns being connected in parallel.

3. Results

3.1. Screening for the most active catalyst

Fig. 1 shows the light-off curves for 9.5MnO_2/HCLT, 9.5CuO/HCLT, 9.5Co_3O_4/HCLT and 9.5Fe_2O_3/HCLT metal oxide catalysts. The lowest T_{50} and T_{90} temperatures were recorded with 9.5MnO_2/HCLT and reported in Table 3. 9.5MnO_2/HCLT was the most active catalyst among the four metal oxides tested. The stability of 9.5MnO_2/HCLT was also studied, which showed a stable activity for over 25 h at toluene combustion temperature of 350 °C, and the conversion of toluene was over 99.5%.

BET surface areas of supported metal oxide catalysts were measured, and listed in Table 1, 9.5MnO_2/HCLT (55 m^2 g^{-1}) < 9.5CuO/HCLT (64 m^2 g^{-1}) < 9.5CoO_2/HCLT (182 m^2 g^{-1}) < 9.5FeO_2/NaCLT (258 m^2 g^{-1}). The activity of MnO_2 supported

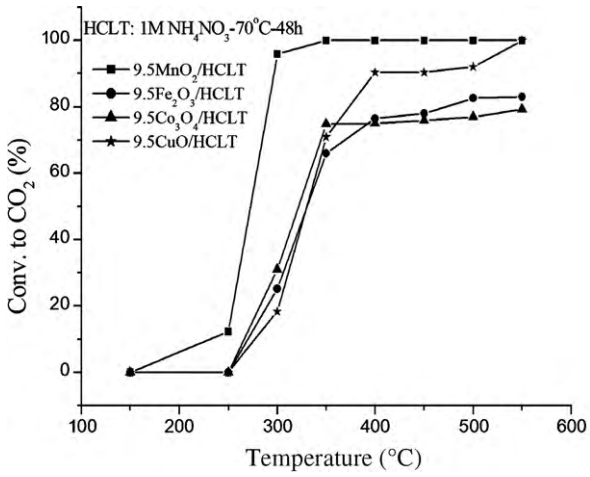

Fig. 1. Light-off curves of combustion of toluene vs. reaction temperature over different catalysts.

Table 4
Surface area and pore properties of the CLT, HCLT and 9.5MnO_2/HCLT.

Catalyst	SSA[a] (m^2/g)	Micropore area (m^2/g)	Micropore volume (cm^3/g)
CLT	39	18	9
HCLT	225	205	107
9.5MnO_2/HCLT	55	12	5

[a] Specific surface area, multi point BET method.

on alternative common zeolites too, i.e., commercial ZSM-5 (9.5/HZSM-5) and BETA (9.5/H-BETA) catalysts were obtained. As shown in Table 2, 9.5MnO_2/HZSM-5 catalyst did not show any noteworthy activity.

Although surface areas of 9.5MnO_2/HZSM-5 and 9.5MnO_2/H-BETA catalysts were comparable and even higher than 9.5MnO_2/HCLT, they did not show higher activity as shown in Table 4. It was clearly seen that the conversion of toluene to CO_2 was much higher with 9.5MnO_2/HCLT catalyst. This finding showed that there was a synergistic effect between 9.5MnO_2 and HCLT support. This point was further clarified by a series of detailed experiments.

The activity of the catalysts is governed by both the adsorption capacity of the catalysts and the strength of the adsorption due to the acidity. During a prolonged ion exchange process in acid medium, the partial dealuminisation of the zeolite framework changes the microporosity. A second variety of larger size micropores might have been developed [22], the total micropore volume is therefore increased and the secondary specific surface area is significantly enlarged [23,24].

Duration of ion exchange changes the adsorption capacity of zeolites, which is directly related to the increasing surface areas as shown in Table 4. Nartural zeolite (CLT) has a surface area of 39 m^2/g. As an example, after 48 h of ion exchange, BET surface area of HCLT has soared to 225 m^2/g. This increased surface area might be due to the removal of acid dissolvable moities in the micropores of natural zeolites. On the other hand, after impregnation, BET surface area of 9.5MnO_2/HCLT has decreased down to 55 m^2/g. This effect may be attributed to the presence of metallic oxides in the poremouths of the zeolitic pores and channels.

3.2. Catalytic tests

3.2.1. Effects of preparation conditions: ion exchangers concentration, ion exchange time and ion exchanger type

It was reported [25] that the activity of the catalysts prepared after 1.5 h long ion exchange with 0.1 M NaCl decreased after reaching to 350 °C. In addition to this study, 6 and 12 h long ion exchange at 30 °C was performed and it was observed that the activity was changed by the ion exchange time. Therefore, we investigated the effects of ion exchange concentration, ion exchange time and ion exchanger.

When the activity changes of catalysts were examined, at the end of the 6 and 12 h ion exchange periods, activity decreased, but by increasing ion exchange periods to even longer durations, such as, 24, 48, 72 h, it was observed that the conversion of toluene to CO_2 increased and then leveled out after 48 h. Catalysts which were prepared after ion exchange with 0.1 M NaCl, and exchanged for 24 and 48 h, did not reach at T_{90} values. After using an ion exchange period of 72 h, it has reached to 100% the conversion of toluene to CO_2 at 500 °C.

Ion exchange process was repeated for 12, 24, 48, and 72 h periods at higher temperature, 70 °C. Following ion exchangers, 1 M NaCl, 1 M NH_4Cl and 1 M NH_4NO_3 were also used for all these periods. In the Fig. 2a, activity change of 9.5MnO_2/NaCLT catalyst prepared with 1 M NaCl was presented. It was observed that T_{50} values were obtained for all catalysts prepared with ion exchange times of 48 and 72 h, T_{90} values have been achieved for the catalysts prepared after ion exchange with NaCl. After ion exchange period of 72 h, 100% the conversion of toluene to CO_2 has been achieved at 500 °C. In Fig. 2b and c, the effect of ion exchange type was presented.

In Fig. 2b, Comparing to the activity pattern of catalysts prepared with NaCl, decrease in the activity after certain temperature was not observed for this ion exchanger. Using the catalysts prepared at the end of the 48 and 72 h ion exchange period, 100% the conversion of toluene to CO_2 was achieved at 350 °C. For all catalysts prepared with NH_4Cl ion exchanger, T_{50} and T_{90} values were observed too.

In Fig. 2c, light-off curves for the catalysts prepared with NH_4NO_3 ion exchanger, were presented. Compared to the NH_4Cl ion exchanger, 100% the conversion of toluene to CO_2 was obtained with 48 h of ion exchange period. Furthermore, the lower T_{50} and T_{90} values were obtained.

Metal oxide catalysts with NH_4NO_3 ion exchanger at 70 °C and 48 h ion exchange time were compared. The maximum conversion of toluene to CO_2 and T_{50}, T_{90} and T_{100} values are listed in Table 3.

3.2.2. Effect of metal oxide loading

The performance of MnO_2/HCLT catalysts with varying MnO_2 loadings was also studied. T_{50} and T_{90} values are listed in Table 3.

The combustion efficiency increased with increasing MnO_2 content up to 9.5%, above which activity remained relatively constant at maximum conversion. At the best conditions, the conversion of toluene to CO_2 was 90% at 292 °C, which was the lowest value attained.

This finding proved that the increase of activity was actually caused by increasing MnO_2 loading and hence this findings lead us to the conclusion of that the activity was provided by MnO_2 or MnO_2 related species. The increased activity was also followed by the increase in weak acid sites, as listed in Table 5. Moreover, there was a similar pronounced relationship between medium + strong acid sites concentration and catalytic activity (Table 3). The highest acid site concentration and activity was for 9.5MnO_2/HCLT catalyst.

It was clearly seen that higher loading of manganese oxide above 9.5 wt.% lead to a decrease in activity. T_{50} temperature of 12MnO_2/HCLT was 6 °C below of that of 9.5MnO_2/HCLT. This difference was further widened to 92 °C for T_{90} values.

9.5% MnO_2 loading on clinoptilolite was taken as an optimum value in the combustion reaction of toluene.

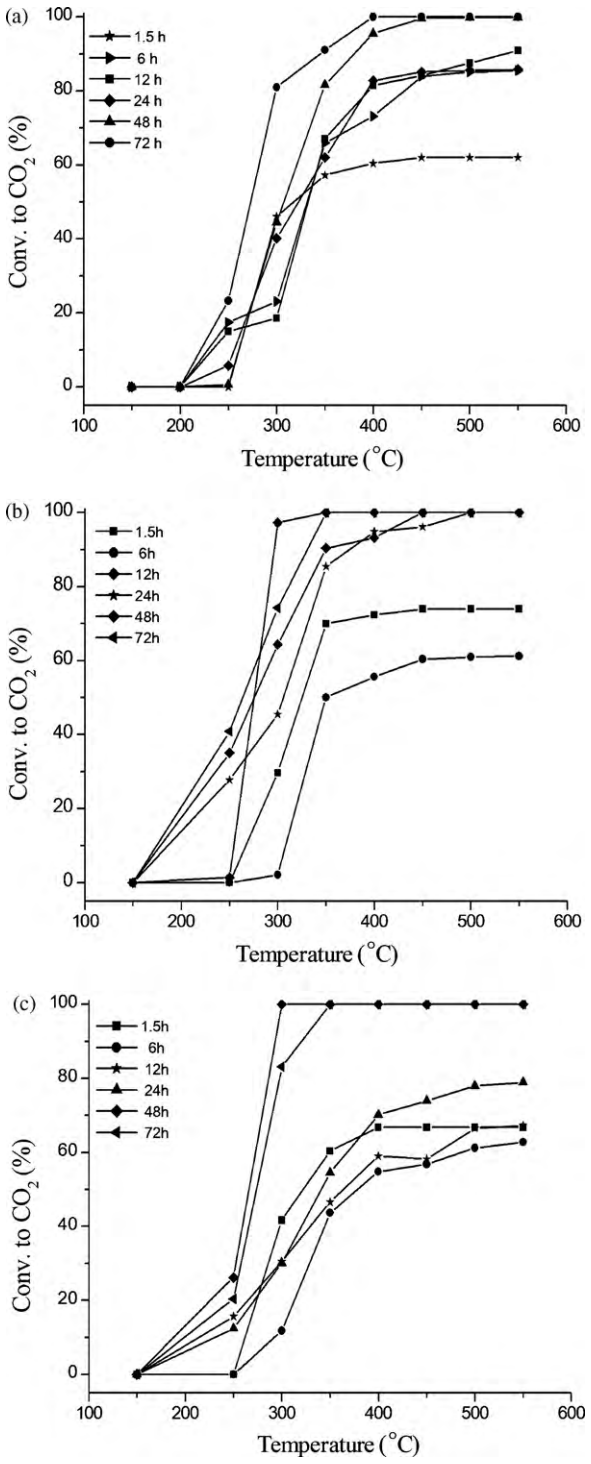

Fig. 2. (a) Toluene conversion vs. reaction temperature over 9.5MnO_2/NaCLT catalyst prepared at various shaking times with 1 M NaCl at 70 °C. (b) Toluene conversion vs. reaction temperature over 9.5MnO_2/HCLT catalyst prepared at various shaking times with 1 M NH_4Cl at 70 °C. (c) Toluene conversion vs. reaction temperature over 9.5MnO_2/HCLT catalyst prepared at various shaking times with 1 M NH_4NO_3 at 70 °C.

3.3. Characterization results

3.3.1. X-ray powder diffraction results

Clinoptilolite was the major crystalline phase detected on the X-ray diffraction pattern as shown in Fig. 3. XRD peaks of clinoptilolite sample and clinoptilolite support in H form were found to be in good agreement with the data of clinoptilolite, JCPDS card

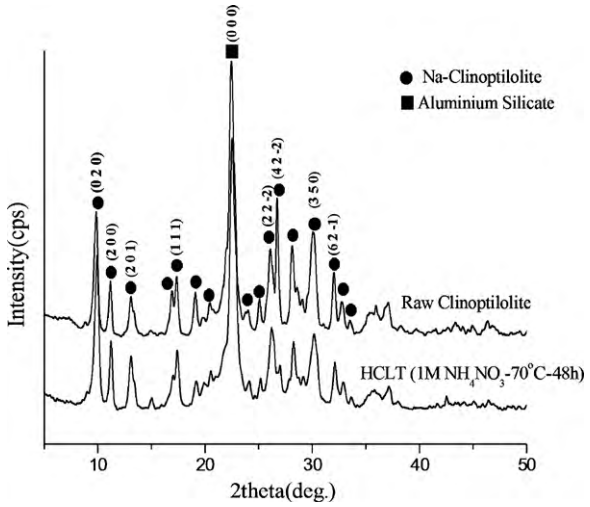

Fig. 3. XRD patterns of the raw clinoptilolite and clinoptilolite support in H form.

(47-1870). In addition to zeolitic and aluminum silicate phases, quartz, cristobalite, and K-feldspar in minor quantities were also detectable in X-ray diffraction patterns. The clinoptilolite content of the sample was estimated to be higher than 85% (w/w).

The diffraction patterns of various metal oxides impregnated clinoptilolite catalysts were obtained. In XRD patterns, the diffraction pattern of crystalline orthorhombic Fe_2O_3 (JCPDS 52-1449), Cubic Co_3O_4 (JCPDS 42-1467), tetragonal MnO_2 (JCPDS 44-0141) and monoclinic CuO (JCPDS 48-1584) were detected. As the MnO_2 content increased, MnO_2 peaks became more apparent whereas, for 3% MnO_2 loaded sample, peaks of MnO_2 were not visible. Crystallinity and crystallite sizes of oxide phases in samples were calculated and listed in Table 2. Metal oxide crystallite size, % crystallinity and weight loss increased as metal oxide content increased.

3.3.2. Temperature-programmed reduction (TPR) and oxidation (TPO)

The reducibility of Mn sites in clinoptilolite was studied by H_2-TPR. These measurements allowed us to estimate the reducibility of metal oxide species, which depended on the interactions with exchanged zeolites framework. TPR profiles of used and fresh catalysts were carried out. 9.5MnO_2/HCLT catalyst showed two reduction peaks at 372 and 458 °C, whereas used 9.5MnO_2/HCLT catalyst showed also two peaks at 392 and 465 °C. The presence of two consecutive peaks at relatively same temperatures clearly demonstrated that the catalyst was not reduced and also oxide structure survived even after the reaction temperature reached at 550 °C. Furthermore, the reduction temperatures of used 9.5MnO_2/HCLT catalyst are the same as calcined 9.5MnO_2/HCLT catalyst.

TPR profiles of the prepared MnO_2/HCLT catalysts with different manganese loadings were also obtained (Fig. 4). The reduction levels of the catalysts were influenced by MnO_2 loading. MnO_2 catalysts showed a two-step reduction process: $MnO_2 \rightarrow Mn_3O_4 \rightarrow MnO$ [26,27].

The TPR profile of 3MnO_2/HCLT showed two broad peaks at about 360 and 460 °C, indicating that manganese over 3MnO_2/HCLT was present as highly dispersed clusters or as isolated manganese ions which interacted strongly with the support. Each sample of 5MnO_2/HCLT, 9.5MnO_2/HCLT, 12MnO_2/HCLT and 20MnO_2/HCLT showed a two-step reduction process, which indicated that the manganese phase of these samples was in the form of bulk like manganese oxide particles with a low interaction with the support surface. As the manganese loading increased, the reduction peak areas became larger and broader, possibly indicating the increase

Table 5
Density of zeolite acid sites, ΔT = temperature range between *n*-butyl amine (NBA) desorbed, δ, is calculated and δ = acidity in mmol NBA/g_{cat}.

Catalysts (metal oxide/zeolite)	Weak sites		Medium + strong sites		δ_{total} (mmol/g_{cat})
	ΔT (°C)	δ (mmol/g_{cat})	ΔT (°C)	δ (mmol/g_{cat})	
3MnO_2/HCLT	56–245	0.462	300–801	0.432	0.894
5MnO_2/HCLT	65–258	0.655	258–792	0.553	1.208
9.5MnO_2/HCLT	70–202	0.749	202–868	0.858	1.607
12MnO_2/HCLT	54–286	0.589	286–761	0.566	1.155
20MnO_2/HCLT	76–244	0.421	244–750	0.395	0.816
9.5CuO/HCLT	83–240	0.734	240–864	0.721	1.455
9.5MnO_2/HZSM-5	33–269	0.761	210–718	1.115	1.876
9.5MnO_2/H-BETA	57–232	0.908	232–627	1.231	2.139
9.5Co_3O_4/HCLT	33–245	0.716	245–801	0.642	1.358
9.5Fe_2O_3/HCLT	42–269	0.702	269–819	0.582	1.284

in active phase. A similar observation was previously reported for manganese-supported catalysts at Mn-loadings from 3.9% to 18.2% [28]. However, a slight shift of TPR peaks to lower temperatures was observed with the sample supported by 12MnO_2/HCLT and 20MnO_2/HCLT. The decrease of reduction temperatures indicated that though small, there was an interaction between MnO_2 and supports.

The reducibility of Cu, Co and Fe sites in exchanged zeolites has also been studied by H_2-TPR. These measurements have been carried out either on parent samples or on exchanged zeolites. Results from H_2-TPR experiments allowed us to estimate the reducibility of metal species. TPR measurements have also been performed on the parent zeolites and on the reference CuO, Co_3O_4 and Fe_2O_3 (the most stable oxides of these metals at the operation conditions) for comparison. TPR profiles are compared in Fig. 5.

As shown in Fig. 5, 9.5CuO/HCLT catalyst showed two reduction peaks at 273 and 307 °C, respectively, corresponding to the two-step reduction: $Cu^{2+} \rightarrow Cu^{1+}$ and $Cu^{1+} \rightarrow Cu^0$ in TPR profile [29,30].

9.5Co_3O_4/HCLT catalyst showed one reduction peak at 511 °C. The high-temperature reduction peak was not observed below 650 °C. In line with our findings, it was reported in the literature [31]. Co_3O_4 gives two TPR peaks at 694 and 757 °C, respectively, corresponding to the two-step reduction: $Co^{3+} \rightarrow Co^{2+}$ and $Co^{2+} \rightarrow Co^0$.

The reduction of 9.5Fe_2O_3/HCLT presents, two-stage reductions, at 392 and at 560 °C, respectively, corresponding to the two-step reduction: $Fe^{3+} \rightarrow Fe^{2+}$ and $Fe^{2+} \rightarrow Fe^0$ [32].

These results suggested that added metal oxides were located on the surface since the reduction temperatures observed was similar to the reduction temperatures of oxides alone. It was reported that iron oxides (or at least an important fraction of it) presents only slight interaction with the zeolite framework [31].

Comparison of 9.5MnO_2/HCLT, 9.5MnO_2/H-BETA and 9.5MnO_2/HZSM-5 catalysts were executed, the TPR profile of 9.5MnO_2/HZSM-5 showed two peaks at about 318 and 450 °C. 9.5MnO_2/H-BETA showed two peaks at 370 and 462 °C and the reduction behavior was like the reduction of 9.5Mn/HCLT catalyst. The areas under these two reduction peaks were much lower for 9.5MnO_2/H-BETA and 9.5MnO_2/HZSM-5 catalysts than that of 9.5MnO_2/HCLT.

The reoxidation of reduced 9.5MnO_2/HCLT catalyst was studied by temperature-programmed oxidation, TPO. The results from TPO experiment are listed in Table 2. TPO profile showed that temperatures where oxidation was occurred were in line with TPR profile. TPO profile of 9.5MnO_2/HCLT catalyst showed two peaks at 365 and 449 °C representing oxygen consumption during the process. The result showed that the stepwise backward oxidation of metallic MnO to MnO_2 occurred. However, the oxidation temperatures decreased and also shifted to lower temperature after reduction process. When O_2 consumption values of catalysts were considered, it was observed that reduced 9.5MnO_2/HCLT catalyst has consumed O_2 at a value which is half of hydrogen consumption value. This has lead us to conclude that the 9.5MnO_2/HCLT catalyst was better in reduction/oxidation cycle that other catalysts.

3.3.3. Acidity measurements

3.3.3.1. Surface acidity measurements. DRIFT (Diffuse Reflectance Fourier Transform Infrared) spectra of ammonia adsorbed on 9.5MnO_2/HCLT at different temperatures are shown in Fig. 6. The spectra showed absorption bands for Lewis and Brønsted acid sites in 9.5MnO_2/HCLT catalyst. The peaks at 1280 and 1632 cm^{-1} were

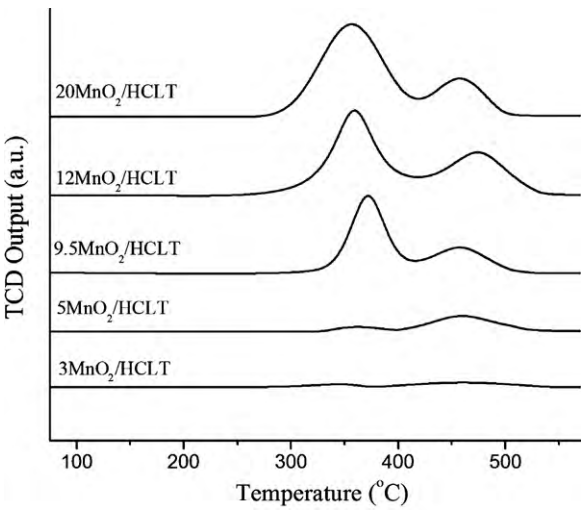

Fig. 4. The TPR profiles of the MnO_2/HCLT catalysts with different manganese loadings.

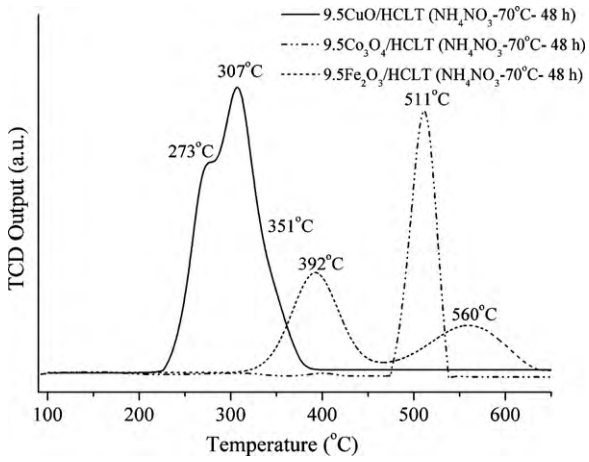

Fig. 5. TPR profiles of 9.5CuO/HCLT, 9.5Co_3O_4/HCLT and 9.5Fe_2O_3/HCLT catalysts.

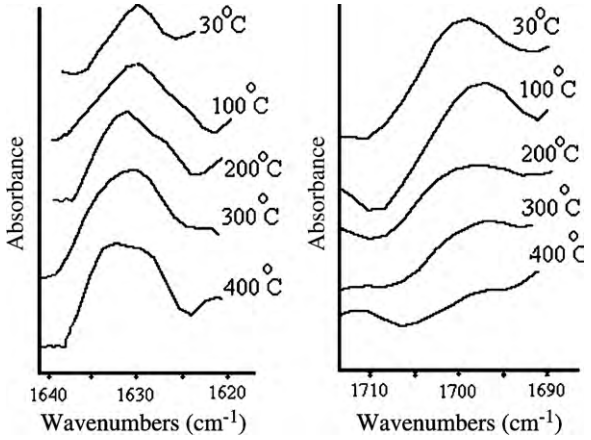

Fig. 6. DRIFT-IR spectra of ammonia adsorbed on nanoscale 9.5MnO_2/HCLT in flowing 5%NH_3/He at 100 °C for 30 min and then purged by He at 30, 100, 200, 300, 400 °C.

taken as an indication of the Lewis acid sites. Peaks appeared at 1470 and 1705 cm^{-1} corresponded to NH_4^+ chemisorbed on the Brønsted acid sites [33,34]. Intense peaks of Lewis sites at 1632 cm^{-1} and Brønsted sites at 1705 cm^{-1} are depicted in Fig. 6.

Brønsted and Lewis acid sites were measured as the integrated areas of corresponding peaks. It was found that Lewis acid sites were more than Brønsted acid sites. With increasing temperatures, the intensities of 1630 cm^{-1} band increased while the intensities of the 1705 cm^{-1} band decreased. This result indicated that some NH_3 species have desorbed and some of NH_4^+ species were transformed to coordinately adsorbed NH_3 on 9.5MnO_2/HCLT. Under typical operating conditions of toluene combustion reaction where maximum activities observed, Brønsted acid sites were not effective in total combustion reaction, whereas Lewis acid sites were in effect.

3.4. Total acidity measurements

Since DRIFT experiments did not lead to quantitative conclusions due to its qualitative nature, we referred to a quantitation of acid sites concentration. In amine adsorption method on acid sites of solid catalysts, the use of *n*-butylamine as molecular probe for the characterization of catalysts has been reported and well established [35,36].

DTG desorption curves of *n*-butylamine were obtained for various catalysts. Based on weight loss values of *n*-butylamine treated catalysts, amount of adsorbed *n*-butylamine was calculated quantitatively. As shown in Table 5, catalysts had three distinct desorption steps depending on their acidity. These were the desorption of physiosorbed *n*-butylamine before 117 °C, dissociation of *n*-butylamine from medium acid sites of the catalysts indicated by the second peak in DTG curves at about 300 °C and dissociation of the *n*-butylamine from strong acid sites of the catalysts indicated by the third peaks in the curves between 483–979 °C. 9.5MnO_2/HCLT had the highest peak intensity in total acid sites. All catalysts had varying degrees of weak, medium and strong acidity. As shown in Table 3 acidity was found to decrease in following order: 9.5MnO_2/HCLT > 9.5CuO/HCLT > 9.5Co_3O_4/HCLT > 9.5Fe_2O_3/HCLT. Surface acidity plays a key role on the activity of acidic catalysts, since the oxidation of hydrocarbons was initiated by the adsorption of the hydrocarbons on these sites by proton transfer [35,37].

The results showed that total surface acidity of samples was changed with the loading of MnO_2. It was observed that total surface acidity was increased as MnO_2 content increased from 3% to 9.5%. On the other hand, when MnO_2 loading increased from 9.5% to 20%, it was observed that there was a reduction in the amount of acid sites. According to the activity results, the reduction in acid sites observed in 20MnO_2/HCLT catalyst was compatible with the activity reduction observed in 20MnO_2/HCLT catalyst. In fact, a decrease in the acidity could probably be explained by partial blocking of the acid sites of support due to the formation of larger MnO_2 particles at higher MnO_2 loadings. Addition to this result, tendency of MnO_2 to form larger particles on zeolite surface has also caused to lower the conversion of toluene to CO_2.

As discussed in acidity results, BETA had more acidity and effective catalyst for toluene combustion in respect to ZSM-5 but it has linear pores that can be rapidly blocked by carbon deposition due to its high acidity [38].

Our results on deposited coke amount of catalysts showed that relatively less carbon deposition occurred over ZSM-5 type zeolite.

The amount of coke over used catalysts was also measured from the weight losses of samples recorded under flowing air in TGA. In pyrolysis run, coke and catalysts were remained, however only catalysts remained in the thermal degradation run in oxidative conditions (air atmosphere). Coke amounts, calculated from comparing the TGA run recorded at heating rate of 10 °C/min under air with the pyrolysis run at the same heating are 2.31% over 9.5MnO_2/H-BETA and 1.33% over 9.5MnO_2/HZSM-5. For 9.5MnO_2/HCLT catalyst, it is observed that the weight losses of calcined and used catalysts were almost zero. It confirmed no coke formation occurred during total combustion of toluene over 9.5MnO_2/HCLT.

4. Conclusions

In this study, we examined Mn^{2+}, Co^{2+}, Fe^{3+}, Cu^{2+} oxides supported on clinoptilolite modified by three ion exchangers in the catalytic combustion of toluene. Favorable higher activities and considerable lowering in T_{50} and T_{90} temperatures have been obtained in terms of toluene conversion with increasing ion exchange time, ion exchange temperature and ion exchanger concentration. The best catalytic activity occurred at the end of the 48 h ion exchanging with NH_4NO_3.

Catalysts containing nitrates of alkaline metals Co, Fe, Mn and Cu were prepared by incipient wetness impregnation of HCLT. The order of activity was found to be: 9.5MnO_2/HCLT > 9.5CuO/HCLT > 9.5Co_3O_4/HCLT > 9.5Fe_2O_3/HCLT. Increase in activity of MnO_2/HCLT catalyst was paralleled by increasing metal oxide content up to 9.5% of MnO_2 loading. Screening of metal oxide catalyst revealed that manganese oxide was the most active catalyst for the combustion of toluene. Furthermore, the lowest T_{50} and T_{90} values were obtained over 9.5MnO_2/HCLT catalyst. With use of 9.5MnO_2/HCLT catalyst, complete oxidation of toluene was achieved at a temperature of as low as 292 °C. The higher catalytic activity of 9.5MnO_2/HCLT catalyst was attributed to a higher acidity of 9.5MnO_2/HCLT, which was enhanced by MnO_2 incorporation. DRIFT-IR measurements of adsorbed ammonia revealed that Lewis acidity played a dominant role in determining the catalytic activity of catalyst.

HCLT type zeolite not only facilitated the combustion but also lowered on-set of combustion. Manganese oxides impregnated HCLT support showed unusually high catalytic combustion activity for the oxides catalysts reported in open literature.

Acknowledgements

This work was supported by TÜBİTAK-ÇAYDAG for the financial support within the research project 107Y096 [2007–2009].

References

[1] K. Everaert, J. Baeyens, Catalytic combustion of volatile organic compounds, J. Hazard. Mater. B109 (2004) 113–139.

[2] H.L. Tidahy, S. Siffert, F. Wyrwalski, J.-F. Lamonier, A. Aboukäıs, Catalytic activity of copper and palladium based catalysts for toluene total oxidation, Catal. Today 119 (2007) 317–320.
[3] M.F. Ribeiro, J.M. Silva, S. Brimaud, A.P. Antunes, E.R. Silva, A. Fernandes, P. Magnoux, D.M. Murphy, Improvement of toluene catalytic combustion by addition of cesium in copper exchanged zeolites, Appl. Catal. B: Environ. 70 (2007) 384–392.
[4] J.J. Spivey, Complete catalytic oxidation of volatile organics, Ind. Eng. Chem. Res. 26 (1987) 2165–2180.
[5] D.R. Van der Vaart, M.W. Vatavuk, A.H. Wehe, Thermal and catalytic incinerators for the control of VOCs, J. Air Waste Manage. Assoc. 41 (1991) 92–98.
[6] M.F. Luo, M. He, Y.-L. Xie, P. Fang., L.-Y. Jin, Toluene oxidation on Pd catalysts supported by CeO_2–Y_2O_3 washcoated cordierite honeycomb, Appl. Catal. B: Environ. 69 (2006) 213–218.
[7] M. Alifanti, M. Florea, V.I. Pârvulescu, Ceria-based oxides as supports for $LaCoO_3$ perovskite; catalysts for total oxidation of VOC, Appl. Catal. B: Environ. 70 (2007) 400.
[8] J. Carpentier, J.F. Lamonier, S. Siffert, E.A. Zhilinskaya, A. Aboukaïs, Characterisation of Mg/Al hydrotalcite with interlayer palladium complex for catalytic oxidation of toluene, Appl. Catal. A: Gen. 234 (2002) 91–101.
[9] R.A. Dalla Beta, Catalytic combustion gas turbine systems: the preferred technology for low emissions electric power production and co-generation, Catal. Today 35 (1997) 129–135.
[10] C. Barbante, A. Veysseyre, C. Ferrari, K. Van de Velde, C. Morel, G. Capodaglio, P. Cescon, G. Scarponi, C. Boutron, Greenland snow evidence of large scale atmospheric contamination for platinum, palladium, and rhodium, Environ. Sci. Technol. 35 (2001) 835–839.
[11] M.C. Alvarez-Galvan, V.A.D.P. O'Shea, J.L.G. Fierro, et al., Alumina-supported manganese- and manganese–palladium oxide catalysts for VOCs combustion, Catal. Commun. 4 (5) (2003) 223–228.
[12] M. Zimowska, A. Michalik-Zym, R. Janik, T. Machej, J. Gurgul, R.P. Socha, J. Podobinïski, E.M. Serwicka, Catalytic combustion of toluene over mixed Cu–Mn oxides, Catal. Today 119 (2007) 321–326.
[13] W.B. Li, M. Zhuang, J.X. Wang, Catalytic combustion of toluene on Cu–Mn/MCM-41 catalysts: influence of calcination temperature and operating conditions on the catalytic activity, Catal. Today 137 (2008) 340–344.
[14] B. Wichterlová, J. Dědeček, Z. Sobalík, in: M.M.J. Treacy, B.K. Marcus, M.E. Bisher, J. Higgins (Eds.), Proceedings of the 12th International Zeolite Conference, vol. 2, Mater. Res. Soc. (1999) 941–973.
[15] A. Corma, M.T. Navarro, From micro to mesoporous molecular sieves: adapting composition and structure for catalysis, Stud. Surf. Sci. Catal. 142 (2002) 487–501.
[16] M.A. Jama, H. Yücel, Equilibrium studies of sodium–ammonium. Potassium–ammonium and calcium–ammonium exchanges on clinoptilolite zeolite, Sep. Sci. Technol. 24 (15) (1989) 1393–1415.
[17] A. Langella, M. Pansini, P. Cappelletti, B. de Gennaro, M. de Gennaro, C. Colella, NH^{4+}, Cu^{2+}, Zn^{2+}, Cd^{2+} and Pb^{2+} exchange for Na^+ in a sedimentary clinoptilolite, Micropor. Mesopor. Mater. 37 (2000) 337–343.
[18] J.C. Miranda-Trevino, C.A. Coles, Kaolinite properties, structure and influence of metal retention on pH, Appl. Clay Sci. 23 (2003) 133–139.
[19] H. Tanaka, N. Yamasaki, M. Muratani, R. Hino, Structure and formation process of (K, Na)-clinoptilolite, Mater. Res. Bull. 38 (2003) 713–722.
[20] M. Ferrandon, E. Bjornbom, Hydrothermal stabilization by lanthanum of mixed metal oxides and noble metal catalysts for volatile organic compound removal, J. Catal. 200 (1) (2001) 148–159.
[21] M. Daturi, G. Busca, G. Groppi, P. Forzatti, Preparation and characterisation of $SrTi_{1-x-y}Zr_xMn_yO_3$ solid solution powders in relation to their use in combustion catalysis, Appl. Catal. B: Environ. 12 (4) (1997) 325–337.
[22] F.M. Bobonich, Yu.G. Voloshina, E.E. Knyazeva, V.G. Voloshinets, Sorption of double-charged cations. Hard and soft acids – by Zeolites, Russ. J. Appl. Chem. 71 (1) (1998) 62–65.
[23] Gr. Mihaila, H.C. Barbu, D. Lutic, M.-I. Sava, Adsorption of sulphur dioxide on clinoptilolite volcanic tuff, in: G. Kirov, L. Filizova, O. Petrov (Eds.), Natural Zeolites-Sofia'95, Pensoft Publ., Sofia-Moskow, 1997, pp. 146–152.
[24] G.E. Christidis, D. Moraetis, E. Keheyan, L. Akhalbedashvili, N. Kekelidze, R. Gevorkyan, H. Yeritsyan, H. Sargsyan, Chemical and thermal modification of natural HEU-type zeolitic materials from Armenia, Georgia and Greece, Appl. Clay Sci. 24 (2003) 79–91.
[25] Z. Özçelik, G.S. Pozan Soylu, İ. Boz, Catalytic combustion of toluene over Mn, Fe and Co-exchanged clinoptilolite support, Chem. Eng. J. 155 (2009) 94–100.
[26] J.I. Gutıerrez-Ortiz, R. Lopez-Fonseca, U. Aurrekoetxea, J.R. Gonzalez-Velasco, Low-temperature deep oxidation of dichloromethane and trichloroethylene by H-ZSM-5-supported manganese oxide catalysts, J. Catal. 218 (2003) 148–154.
[27] M.F. Luo, X.X. Yuan, X.M. Zheng, Catalyst characterization and activity of Ag–Mn, Ag–Co and Ag–Ce composite oxides for oxidation of volatile organic compounds, Appl. Catal. A 175 (1–2) (1998) 121–129.
[28] M.C. Álvarez-Galváan, B. Pawelec, V.A. de la Peñna O'Shea, J.L.G. Fierro, P.L. Arias, Formaldehyde/methanol combustion on alumina-supported manganese-palladium oxide catalyst, Appl. Catal. B: Environ. 51 (2) (2004) 83–91.
[29] A.P. Antunes, M.F. Ribeiro, J.M. Silva, F.R. Ribeiro, C.P. Magnoux, M. Guisnet, Catalytic oxidation of toluene over CuNaHY zeolites: coke formation and removal, Appl. Catal. B: Environ. (33) (2001) 149–164.
[30] M.F. Ribeiro, J.M. Silva, S. Brimaud, A.P. Antunes, E.R. Silva, A. Fernandes, P. Magnoux, D.M. Murphy, An investigation of a new regeneration method of commercial aged three-way catalysts, Appl. Catal. B: Environ. 65 (2006) 93–100.
[31] E. Díaz, S. Ordónez, A. Vega, J. Coca, Catalytic combustion of hexane over transition metal modified zeolites NaX and CaA, Appl. Catal. B: Environ. 56 (2005) 313–322.
[32] G. Qi, R.T. Yang, Ultra-active Fe/ZSM-5 catalyst for selective catalytic reduction of nitric oxide with ammonia, Appl. Catal. B: Environ. 60 (2005) 13–22.
[33] N.Y. Topsøe, Characterization of the nature of surface sites on vanadia–titania catalysts by FTIR, J. Catal. 128 (1991) 499–511.
[34] W.S. Kijlstra, D.S. Brands, E.K. Poels, A. Bliek, Mechanism of the selective catalytic reduction of NO by NH_3 over MnO_x/Al_2O_3, J. Catal. 171 (1997) 208–218.
[35] V.J. Fernandes, A.S. Araujo, G.J.T. Fernandes, Thermal analysis applied to solid catalysts acidity, activity and regeneration, J. Therm. Anal. Calorim. 56 (1999) 275–285.
[36] D.R. Milburn, K. Saito, R.A. Keogh, B.H. Davis, Sulfated zirconia: attempt to use *n*-butylamine to measure acidity, Appl. Catal. A: Gen. 215 (2001) 191–197.
[37] R. Lopez-Fonseca, A. Aranzabal, J.I. Gutierrez Ortiz, J.I. Alvarez-Uriarte, J.R. Gonzalez-Velasco, Comparative study of the oxidative decomposition of trichloroethylene over H-type zeolites under dry and humid conditions, Appl. Catal. B 30 (2001) 303–313.
[38] J.W. Park, J.-H. Kim, G. Seo, The effect of pore shape on the catalytic performance of zeolites in the liquid-phase degradation of HDPE, Polym. Degrad. Stab. 76 (2002) 495–501.